Chapter 6

Results and Conclusion

Lacking any evidence for non-Standard Model production of events with large $\not{E}_T$ and multiple jets, the final step in our search is the simulation of the expected signal from squark and gluino production and decay and the extraction of cross section and mass limits from the data. In this chapter we describe the specific model used and the limits we extracted.

6.1 Specification of the Model

The Minimal Supersymmetric Standard Model (as described in Chapter 1) has too many free parameters to allow a fully exhaustive search. Reasonable progress is made by fixing all parameters except the gluino and squark masses. In choosing values for the fixed parameters we were guided by previous experimental searches and the limits they have set. The LEP experiments have essentially excluded squarks and charginos below the kinematic limit of 45 GeV and neutralinos below about 23 GeV [47]. In the MSSM these limits may be transformed into a limit on the gluino mass; the limit depends on the values of μ and $\tan(\beta)$ chosen for the model. The chargino and neutralino limits are weakened by some choices of μ and $\tan(\beta)$. We have chosen values of these parameters which are consistent with existing LEP limits, and have chosen a large value of m_{H^+} as preferred by most theorists. The parameters we fixed were the following:

- $\mu = -250$ GeV.
- $\tan(\beta) = 2.0$,
- $m_{H^+} = 500$ GeV,

The branching fractions for each squark and gluino decay mode are slowly varying functions of these parameters.

To produce signal events we used the generator ISASUSY [48]. ISASUSY is an extension of the generator ISAJET which models the production of squarks and gluinos in $p\bar{p}$ collisions, and their subsequent decay according to the constraints of the MSSM. The version of ISASUSY we used included neither the production of scalar leptons (sleptons) nor scalar top quarks (stop squarks). The exclusion of sleptons is approximately equivalent to setting their mass to be the same magnitude as the squark mass. The exclusion of a separate stop squark means that we are sensitive to the other five squark flavors, but not to the production of the (lighter) stop, which has a different signature than the heavier squarks. Thus our analysis shall not set a limit on the mass of a light stop, but rather on the mass of the heavier squarks.

To calculate cross sections, we used the program SUSYXS, which includes the same code as ISASUSY for the calculation of cross sections but does not generate events. Our version of SUSYXS uses the EHLQ structure function [49]. Since the cross section calculations have been done only to leading order, and since for the production of heavy objects it is the structure function values for large momentum fractions which matter, the choice of structure function parameterization has little impact. What has greater impact for the cross section calculation is the choice of the scale at which α_s is calculated and the factorization scale used for the structure function. SUSYXS uses the same scale for both. Changing the scale from $4\hat{s}$ to $\hat{s}/4$ produces approximately a factor of two change in the production cross section. We have chosen to take a middle value of $\hat{s}$ as the scale for our calculations, and have studied how changing the scale from $4\hat{s}$ to $\hat{s}/4$ alters our results.

6.2 Signal Efficiencies

We generated events for 28 different combinations of $m_{\tilde{q}}$ and $m_{\tilde{g}}$. Each of the samples was analyzed in the same manner as the simulated backgrounds described in Chapter 5. Table 6.1 contains the results of the signal calculations. The table contains, for each signal sample, the gluino and squark masses ($m_{\tilde{g}}$ and $m_{\tilde{q}}$), the total production cross section σ_{tot}, and our detection efficiency $\tilde{\varepsilon}$. The cross section was calculated with SUSYXS using the structure functions and q^2 scale given above. The statistical and systematic errors in $\tilde{\varepsilon}$ were determined in the same manner as described for the background samples.

$m_{\tilde{g}}$	$m_{\tilde{q}}$	σ_{tot} (pb)	$\tilde{\varepsilon}$ (%)	$m_{\tilde{g}}$	$m_{\tilde{q}}$	σ_{tot} (pb)	$\tilde{\varepsilon}$ (%)
100	100	1420	$4.62 \pm 0.68^{+1.39}_{-0.96}$	220	220	7.45	$19.75 \pm 2.04^{+1.37}_{-0.69}$
100	150	630	$1.76 \pm 0.40^{+0.50}_{-0.60}$	221	200	11.7	$18.07 \pm 1.94^{+1.37}_{-0.94}$
100	500	435	$1.20 \pm 0.33^{+0.13}_{-0.26}$	225	300	1.77	$17.17 \pm 1.55^{+1.55}_{-1.55}$
150	100	472	$4.91 \pm 0.70^{+1.25}_{-0.82}$	225	500	1.35	$15.24 \pm 1.76^{+1.55}_{-1.21}$
150	200	50.4	$7.63 \pm 0.91^{+0.89}_{-1.08}$	250	250	2.60	$25.35 \pm 2.38^{+1.03}_{-1.47}$
150	300	28.1	$7.62 \pm 0.92^{+1.10}_{-1.08}$	250	50	4990	$0.26 \pm 0.10^{+0.10}_{-0.00}$
150	400	28.4	$6.30 \pm 0.81^{+1.36}_{-0.74}$	275	275	1.11	$26.97 \pm 2.12^{+1.55}_{-0.65}$
150	500	30.6	$7.54 \pm 1.19^{+1.30}_{-1.39}$	300	150	27.8	$11.67 \pm 1.19^{+1.72}_{-0.86}$
175	300	9.48	$11.56 \pm 1.51^{+1.91}_{-2.17}$	300	200	6.18	$20.06 \pm 2.06^{+1.03}_{-2.14}$
175	500	10.0	$10.31 \pm 1.42^{+1.56}_{-1.56}$	400	100	159	$3.43 \pm 0.78^{+0.86}_{-1.20}$
200	150	53.4	$15.41 \pm 1.43^{+1.55}_{-2.09}$	400	150	21.1	$8.30 \pm 1.25^{+1.93}_{-2.03}$
200	200	15.6	$18.56 \pm 1.62^{+0.77}_{-1.45}$	400	200	4.41	$17.08 \pm 1.53^{+2.00}_{-1.54}$
200	220	10.4	$19.04 \pm 2.01^{+0.51}_{-1.80}$	400	250	1.08	$25.26 \pm 2.02^{+2.06}_{-1.49}$
200	400	3.12	$14.37 \pm 1.37^{+1.38}_{-1.86}$	500	100	143	$1.44 \pm 0.36^{+0.34}_{-0.34}$

Table 6.1: Squark and gluino production cross sections and detection efficiencies for our 28 simulated event samples.

It was impractical to generate event samples on a fine enough mass grid to allow easy determination of our signal detection efficiency for every point in the ($m_{\tilde{g}}$, $m_{\tilde{q}}$) plane. Instead, we used a combination of linear fitting and linear interpolation. We selected four sets of samples:

- all with $m_{\tilde{g}} = 400$ GeV;

- all with $m_{\tilde{q}} = 300$ GeV;

- all with $m_{\tilde{q}} = 500$ GeV;

- all with $m_{\tilde{g}} = m_{\tilde{q}}$;

and fit a straight line to each set to determine the variation of efficiency with squark mass (along the $m_{\tilde{g}} = 400$ GeV line) or gluino mass (along the $m_{\tilde{q}} = 300$ GeV and $m_{\tilde{q}} = 500$ GeV lines) or both (along the $m_{\tilde{g}} = m_{\tilde{q}}$ line). Figure 6.1 contains plots of these efficiencies and the linear fits to the plots. In all cases the quality of the fit was good. The error bars on the points show the statistical errors only; the dotted lines show the systematic errors, determined by repeating the fits for systematically high and low efficiencies as given in Table 6.1.

To determine our efficiency at a point $(m_{\tilde{g}}, m_{\tilde{q}})$ we used linear interpolation between the appropriate bounds from Figure 6.1. We propagated statistical errors with the standard technique, including the effect of the correlation between the slopes and intercepts of the linear fits. We propagated systematic errors by linear interpolation between the high and low systematic fits.

6.3 Cross Section Limits

To determine our cross section limit we first must determine the signal cross section $\tilde{\sigma}$ to which we are sensitive. This is the cross section observed minus the cross section predicted for the backgrounds scaled by our signal efficiency,

$$\tilde{\sigma} = \frac{\Big((N - n_{\text{QCD}})/\mathcal{L}\Big) - \sigma_{\text{vis}}}{\tilde{\varepsilon}}. \tag{6.1}$$

where $N = 14$ is the number of events seen in the data, $n_{\text{QCD}} = 0.42 \pm 0.37$ is our predicted number of events from QCD, $\sigma_{\text{vis}} = 2.46 \pm 0.25^{+1.04}_{-0.97}$ is our

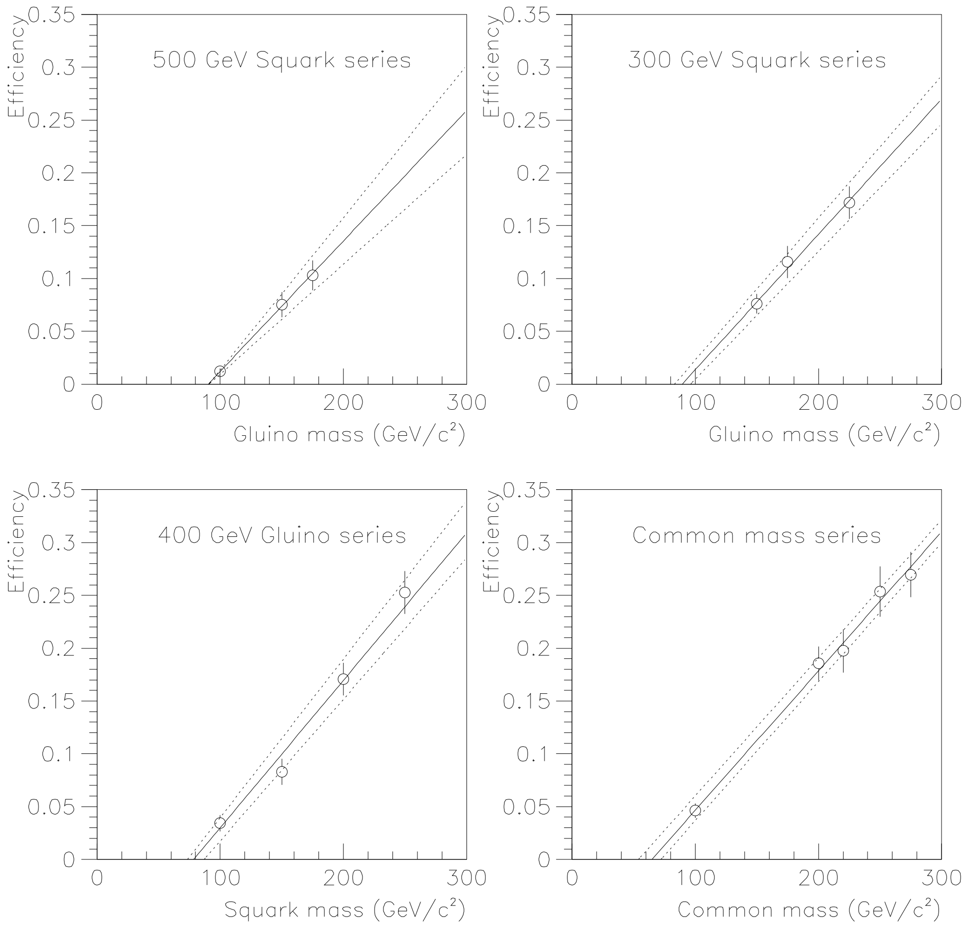

Figure 6.1: The signal efficiencies for selected $(m_{\tilde{g}}, m_{\tilde{q}})$ and the fits used in interpolating between them. The error bars are statistical only. The solid lines are the fits to the nominal efficiencies and the dotted lines show the systematic errors. The values of the fit χ^2 per degree of freedom are, from upper left to lower right, 0.031, 0.20, 1.27, and 0.20.

predicted W and Z background cross section, and $\tilde{\varepsilon}$ is our signal efficiency, which varies with $m_{\tilde{g}}$ and $m_{\tilde{q}}$.

The calculation of the upper limit to any confidence level α from this formula is in theory quite simple. Assuming one knows the (properly normalized) distribution P of $\tilde{\sigma}$, one merely determines what value $\tilde{\sigma}_\alpha$ satisfies the requirement that the probability content of the interval $[0, \tilde{\sigma}_\alpha]$ equals α:

$$\alpha = \int_0^{\tilde{\sigma}_\alpha} P(\sigma)\, d\sigma. \tag{6.2}$$

The difficultly, of course, is in the details. One frequently does not know the distribution governing errors; Gaussian errors are usually assumed. In our case the number of events seen is sufficiently large (14) that we use the Gaussian distribution with width $\sqrt{14}$ rather than the exact Poisson distribution to describe it; we assume all other statistical errors are Gaussian. The Gaussian distribution is not, however, appropriate for the systematic errors.

The decision of how to handle systematic errors in the setting of a limit is sometimes a difficult one. There exists an established theory for the handling of statistical errors, but not for systematic errors, which are *not* statistical. Indeed it is most often the case that one cannot determine an accurate probability content for a systematic error estimate, and that it reflects instead the "reasonable" variation of some parameter, fit method, or choice of model. Some authors, while recognizing that systematic errors are not statistical, decide to handle them in as if they were. We have done this to some extent in our combination of systematic errors leading up to the errors in σ_{vis} and $\tilde{\epsilon}$, although we have taken care that the errors we have combined come from unrelated sources. For our final limit calculation, we prefer to handle the systematic errors in a conservative fashion. For each $(m_{\tilde{g}}, m_{\tilde{q}})$ we compute $\tilde{\sigma}$ four times, allowing each of $\sigma_{\rm vis}$, $\mathcal{L}$ and $\tilde{\varepsilon}$ to vary from its nominal value to it nominal plus and minus one systematic error interval. The energy scale uncertainty influences both $\sigma_{\rm vis}$ and $\tilde{\varepsilon}$; in each calculation we take the error in the same direction for both. We then choose the largest of the calculated values, $\tilde{\sigma}'$, as the conservative central value to be used in the limit calculation, and use the statistical error $\delta\tilde{\sigma}$ as the width of the Gaussian distribution. For the 95% confidence level limit $\tilde{\sigma}_{95\%}$ we solve the equation

$$0.95 = \frac{\int_0^{\tilde{\sigma}_{95\%}} d\sigma \, e^{-\left((\sigma-\tilde{\sigma}')/\delta\tilde{\sigma}\right)^2/2}}{\int_0^{\infty} d\sigma \, e^{-\left((\sigma-\tilde{\sigma}')/\delta\tilde{\sigma}\right)^2/2}} \tag{6.3}$$

for $\tilde{\sigma}_{95\%}$. Since $\tilde{\varepsilon}$ is a function of $m_{\tilde{q}}$ and $m_{\tilde{g}}$ this cross section limit also depends on them. Table 6.2 gives our 95% confidence level cross section limit for various $m_{\tilde{g}}$ and $m_{\tilde{q}}$.

6.4 Mass Limits

To turn our cross section limit into a gluino and squark mass limit we use the calculation of the production cross section obtained with SUSYXS. We merely compare, point by point, our cross section limit with the calculated cross section; if our limit is lower than the calculated cross section, then the point is excluded at the 95% confidence level. As discussed above there is substantial uncertainty (due to the different α_s and factorization scale choices) in the cross section calculation. Figure 6.2 shows the region excluded by our

	$m_{\tilde{g}}$ (GeV)						
$m_{\tilde{q}}(GeV)$	100	150	200	250	300	350	400
100	38.0	41.6	44.9	49.0	53.9	60.2	68.5
150	47.5	14.8	15.2	15.6	16.1	16.6	17.1
200	64.4	16.6	9.2	9.4	9.5	9.7	9.9
250	102.9	19.0	10.4	6.7	6.8	6.9	6.99
300	256.4	22.3	11.9	8.1	5.2	5.3	5.4
350	225.1	22.5	12.1	8.3	6.3	4.3	4.4
400	222.2	22.8	12.3	8.4	6.4	4.6	3.7

Table 6.2: Our 95% confidence level cross section limit (in picobarns) for the production of gluinos and squarks in $p\bar{p}$ collisions at a center of mass energy of 1.8 TeV, as a function of $m_{\tilde{g}}$ and $m_{\tilde{q}}$.

search at the 95% confidence level and the band of uncertainty induced by the cross section error. Henceforth we shall refer to the middle contour as our limit; the reader should keep in mind the approximately ± 10 GeV effect of the cross section uncertainty. The reader should also note that our analysis did not explore the low mass regions (below 100 GeV) except for the one point $m_{\tilde{g}} = 250$ GeV, $m_{\tilde{q}} = 50$ GeV, since most of this region had been excluded by previous experiment.

In the limit of $m_{\tilde{q}} \gg m_{\tilde{g}}$, gluino pair production dominates over the other two processes, and the gluino decay patterns are insensitive to further increase in the squark mass. In this region we produce an asymptotic limit of $m_{\tilde{g}} > 157$ GeV at the 95% confidence level. In the case of equal squark and gluino masses, we produce a limit $m_{\tilde{g}} = m_{\tilde{q}} > 218$ at the 95% confidence level. In the limit of heavy gluinos the model eventually breaks down. Recall that

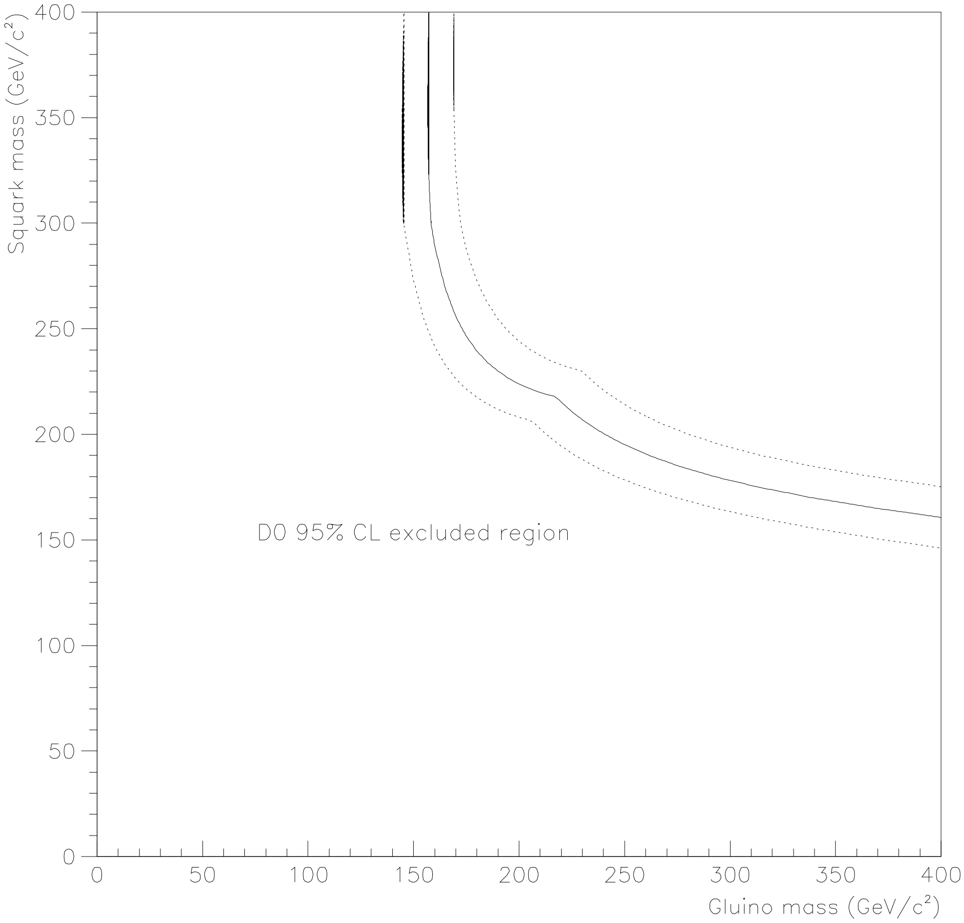

Figure 6.2: The DØ 95% confidence level exclusion contour. The solid line is the result of using an α_s and factorization scale of $\hat{s}$; the upper dotted line is for $\hat{s}/4$ and the lower is for $4\hat{s}$.

the mass of $\tilde{Z}_1$, the LSP, depends on the $m_{\tilde{g}}$. Thus the gluino cannot become too much heavier than the squark, or the squark would become the LSP; the existence of a charged, color-bearing stable squark would have long ago been detected. Before that extreme is reached, the $\tilde{Z}_1$ becomes sufficiently massive that the $\not\!\!E_T$ signal from the decay $\tilde{q} \rightarrow q\tilde{Z}_1$ becomes small, and our signal detection efficiency becomes negligible. Thus for sufficiently heavy gluinos we can set no limit on the squark mass. We have not yet produced any simulated events in this region of the ($m_{\tilde{g}}$, $m_{\tilde{q}}$) plane, and can state only that the gluino mass for which we can set no squark mass limit is above 400 GeV. Although we are confident that our efficiency interpolation is accurate in the regions between our existing simulated signal samples, we do not want to extrapolate the fits beyond the region we have investigated. Evaluation of the sample at $m_{\tilde{g}} = 250$ GeV and $m_{\tilde{q}} = 50$ GeV does allow us to exclude that point at the 95% confidence level; using Equation 6.3 we obtain a 95% confidence level upper limit on the cross section of 340 pb, while the MSSM cross section is in the range 3900–6600 pb, depending on the scale choice. Similarly, the point at $m_{\tilde{g}} = 500$ GeV and $m_{\tilde{q}} = 100$ GeV is excluded; our cross section limit is 57 pb, while the MSSM cross section is in the range 106–193 pb.

6.5 Comparison with Previous Results

Our search was not extended to low squark and gluino masses, since they have already been excluded by previous work. The LEP experiments provide a lower mass limit of 45 GeV for the squark and a gluino mass limit that depends on the choices of $\tan(\beta)$ and μ. CDF provides a gluino mass limit of 30 GeV $\leq m_{\tilde{g}} \leq$ 95 GeV in the limit of heavy squarks for the same choices of $\tan(\beta)$ and μ used in our analysis [50]. Earlier results from UA1 and UA2 did not employ the MSSM, but excluded the ranges 4 GeV $\leq m_{\tilde{g}} \leq$ 53 GeV and 16 GeV $\leq m_{\tilde{g}} \leq$ 79 GeV; in the lower mass regions the assumption that the gluino decays via $\tilde{g} \to q\bar{q}\tilde{\gamma}$ is not far different from the prediction of the MSSM [51, 52]. Searches for the decays $\psi \to \gamma\eta_{\tilde{g}}$ and $\Upsilon \to \gamma\eta_{\tilde{g}}$, where $\eta_{\tilde{g}}$ is the pseudoscalar $\tilde{g}\tilde{g}$ bound state, exclude $m_{\tilde{g}} \leq$ 1 GeV and $m_{\tilde{g}} \leq$ 3 GeV, respectively [53]. The possible existence of a "light gluino window" around 3 GeV is still a matter of dissent. The CDF squark mass limit of reference [50] depends on the mass of gluino, as does our own. CDF sets no squark mass limit when $m_{\tilde{g}}$ is greater than 410 GeV. We have refrained from extending our exclusion contour into the region above $m_{\tilde{g}} =$ 400 GeV because at this time we lack sufficient simulated signal samples in that region; however, the single sample we have at $m_{\tilde{g}} =$ 500 GeV, $m_{\tilde{q}} =$ 100 GeV demonstrates that we can extend existing limits in that region as well. These results are all summarized in Figure 6.3.

6.6 Future Considerations

In the present Tevatron run (Run IB) we expect to collect up to 75 pb^{-1} of integrated luminosity; this will help to extend our search to heavier masses. More important, however, are some improvements of technique.

DØ should soon publish measured cross sections for the process $p\bar{p} \to$

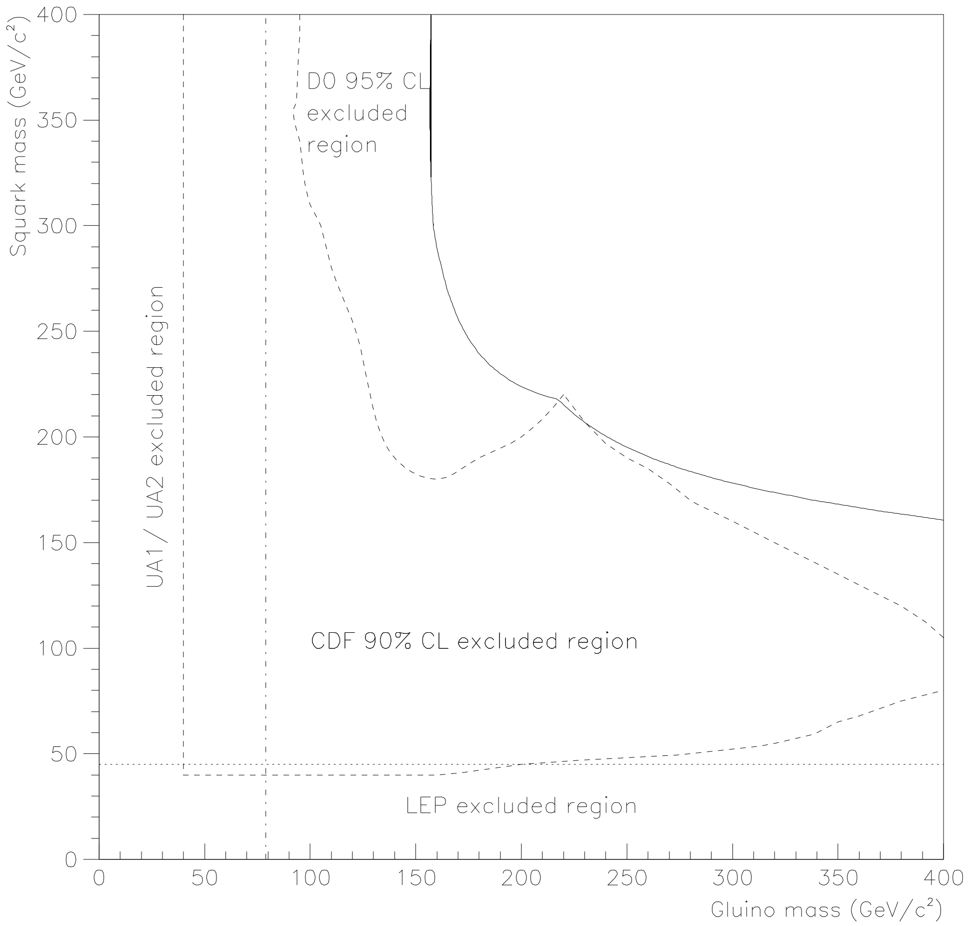

Figure 6.3: Current squark and gluino mass limits. Left of the dot-dashed line is the gluino mass region excluded by UA1 and UA2. Below the dotted line is the squark mass region excluded by the LEP experiments. Inside the dashed line is the CDF 90% confidence level excluded region. Below the solid line is the DØ 95% confidence level excluded region.

$W + n$ jets. Once the analysis on these data is mature, we should be able to avoid the large systematic uncertainties of the Monte Carlo determination of W and Z backgrounds; we may modify the $W \rightarrow e\bar{\nu}$ events by removing the electron to make an event like $Z \rightarrow \nu\bar{\nu}$, or replace the e by a μ or simulated τ.

An increase in both the number and size of simulated signal samples would make interpolation of efficiency easier and reduce the statistical error in the efficiency calculations. To obtain the number and size of samples necessary a new and faster detector simulation, specifically tuned to reproduce DØ's jet and $\not{E}_T$ response, is needed. Extension of our search to heavier masses also requires, of course, producing additional simulated samples at those masses.

The greatest sensitivity to new physics from the MSSM will come from combining results from all the supersymmetry searches underway in the collaboration; searches for charginos and neutralinos, scalar top, and multilepton decays of squarks and gluinos are all underway. And finally, one can hope to see a signal at last, and be faced with the happy problem of determining the masses of the superparticles and testing the theory in more detail.

Bibliography

[1] T.D. Lee, **Symmetries, Asymmetries, and the World of Particles**, p. 57, University of Washington Press (1988).

[2] S. Weinberg, Phys. Rev. Lett **19**, 1264 (1967).

[3] G. Arnison *et al.*, Phys. Lett. **122B**, 103 (1982).

[4] G. Arnison *et al.*, Phys. Lett. **126B**, 398 (1983).

[5] M. Banner *et al.*, Phys. Lett. **122B**, 476 (1983).

[6] P. Bagnaia *et al.*, Phys. Lett. **129B**, 130 (1983).

[7] G. Ross, **Grand Unified Theories**, Benajamin/Cummings (1984).

[8] Y. Golfand and E. Likhtman, JETP Lett. **13**, 323 (1971).

[9] D. Volkov and V. Akulov, Phys. Lett. **46B**, 109 (1973).

[10] J. Wess and B. Zumino, Nucl. Phys. **B70**, 39 (1974).

[11] X. Tata, in **The Standard Model and Beyond**, p. 304, ed. J. Kim, World Scientific, Singapore (1991); H. Nilles, Phys. Rep. **110**, 1 (1984);

P. Nath, R. Arnowitt, and A. Chamseddine, **Applied N=1 Supergravity** (ICTP Series in Theoretical Physics, Vol. 1), World Scientific, Singapore (1984); H. Haber and G. Kane, Phys. Rep. **117**, 75 (1985).

[12] H. Baer, M. Drees, and X. Tata, Phys. Rev. **D41**, 3414 (1990).

[13] H. Baer *et al.*, Phys. Lett. **161B**, 175 (1985).

[14] H. Baer, V. Barger, D. Karatas, and X. Tata, Phys. Rev. **D36**, 96 (1987).

[15] H. Baer, X. Tata, and J. Woodside, Phys. Rev. **D41**, 906 (1990).

[16] U.Amaldi *et al.*, Phys. Lett. B 281 (1992).

[17] W. Thompson, State University of New York at Stony Brook, Ph. D. Thesis, *Search for the Top Quark in the Muon + Jets Channel at D0* (1994) (unpublished).

[18] S. Abachi *et al.*, Nucl. Inst. and Meth., **A338**, (1993).

[19] D. Perkins, **Introduction to High Energy Physics, 2nd Edition**, Benjamin/Cummings (1982).

[20] M. Abolins *et al.*, Nucl. Instr. and Methods, **A280**, 36 (1989).

[21] S. Abachi *et al.*, Nucl. Instr. and Methods, bf A324, 53 (1993).

[22] J. Linnemann, in "Proceedings of the American Physical Society Division of Particles and Fields Conference", Fermilab (Nov. 1992), ed. R. Raja and J. Yoh.

[23] M. Abolins *et al.*, IEEE Trans. Nuc. Sci. **36**, No. 1 (1989).

[24] M. Fortner *et al.*, IEEE Trans. Nuc. Sci. **38** (1991).

[25] M. Paterno, DØ Internal Note 1782 (1993) (unpublished).

[26] R. Engelmann *et al.*, Nucl. Instr. and Methods **216**, 45 (1983).

[27] M. Narain, in "Proceedings of the American Physical Society Division of Particles and Fields Conference", Fermilab (Nov. 1992), ed. R. Raja and J. Yoh.

[28] U. Heintz and M. Narain, DØ Internal Note 1814 (1993) (unpublished).

[29] N. Hadley, DØ Internal Note 904 (1989) (unpublished).

[30] M. Paterno, DØ Internal Note 1374 (1992) (unpublished).

[31] The CDF Collaboration, F. Abe *et al.*, Phys. Rev. Lett. **69**, 2896 (1992).

[32] J. Bantly and Q. Li-Demarteau, DØ Internal Note 1691 (1993) (unpublished).

[33] J. Bantly, DØ Internal Note 1849 (1993) (unpublished).

[34] N. Amos, J. Linnemann, R. Partridge and L. Paterno, DØ Internal Note 2031 (1994) (unpublished).

[35] R. Astur, private communication.

[36] V. D. Elvira, J. Blazey, and R. Astur, DØ Internal Note 1763 (1993) (unpublished).

[37] M. Bhattacharjee, private communication.

[38] C. Gerber, P. Quintas, and D. Wood, DØ Internal Note 1718 (1993) (unpublished).

[39] C. Gerber, P. Quintas, and D. Wood, DØ Internal Note 1904 (1993) (unpublished).

[40] C. Gerber, private communication.

[41] F. Berends, W. Geile, H. Kuijf, and B. Tausk, FERMILAB-Pub-90/213-T (1990).

[42] F. Paige and S. Protopopescu, Brookhaven National Laboratory Report BNL-37066 (1985) (unpublished).

[43] W. Dharmaratna, R. Raja, and C. Stewart, DØ Internal Note 1730 (1993) (unpublished).

[44] R. Brun and F. Carminati, "GEANT Detector Description and Simulation Tool," CERN, CERN Program Library Long Writeup W5013 (1993).

[45] "D0$LEVEL1:L1SIM.DOC," DØ Online documentation.

[46] Phys. Rev. **D45**, "Review of Particle Properties".

[47] T. Medcalf, "The Search for Supersymmetry with the Aleph Detector at LEP"; P. Lutz, "SUSY with DELPHI"; B. Zhou, "Results of Supersymmetric Particle Searches with the L3 Detector"; R. Brown, "Searches for

New Particles in OPAL"; all in **International Workshop on Supersymmetry and Unification of Fundamental Interactions**, P. Nath ed., World Scientific, Singapore (1993).

[48] ISASUSY was written by H. Baer and X. Tata, and is an extension of ISAJET by F. Paige and S. Protopopescu. The physics included in ISASUSY was incorported into ISAJET in ISAJET 7.0.

[49] K. Ellis *et al.*, FERMILAB-Pub-86/75-T (1986).

[50] F. Abe *et al.*, Phys. Rev. Lett. **69** (1992).

[51] C. Albajar *et al.*, Phys. Lett **B198** (1987).

[52] J. Alitti *et al.*, Phys. Lett. **B235** (1990).

[53] J. Lee-Franzini, in "Supernova 1987A, One Year Later: Results and Perspectives in Particle Physics", in **Proceedings of Les Rencontres de Physique de la Valee d'Aosta**, M. Greco, ed., Editions Frontieres, Gif-sur-Yvette, France (1988).